Challenges in Panchromatic Modelling with Next Generation Facilities
Proceedings IAU Symposium No. 341, 2018
M. Boquien, E. Lusso, C. Gruppioni & P. Tissera, eds.

doi:10.1017/S1743921319002175

FIRSTLIGHT: Cosmological simulations of first galaxies at cosmic dawn

Daniel Ceverino

Universitat Heidelberg, Zentrum für Astronomie, Institut fur Theoretische Astrophysik, Albert-Ueberle-Str. 2, 69120 Heidelberg, Germany

Abstract. Using the FirstLight database of 300 zoom-in cosmological simulations we provide rest-frame UV-optical spectral energy distributions of galaxies with complex star-formation histories that are coupled to the non-uniform gas accretion history of galactic halos during cosmic dawn. The population at any redshift is very diverse ranging from starbursts to quiescent galaxies even at a fixed stellar mass. The FirstLight simulations make predictions on the rest-frame UV-optical absolute magnitudes, colors and optical emission lines of galaxies at $z = 6 - 12$ that will be observed for the first time with JWST and the next generation of telescopes in the coming decade.

Keywords. galaxies: evolution – galaxies: formation – galaxies: high-redshift

1. Introduction

The period of cosmic dawn, the first billion years in the history of the Universe, is the final frontier for galaxy formation. Theory roughly predicts that the first galaxies form in the first gravitationally bound structures at high redshifts, $z \geqslant 12$. They quickly start to ionize their surroundings, driving the reionization of the Universe, which ends around $z \simeq 6$. However, little is known about these primeval galaxies. One of their most important properties is their spectral energy distribution (SED). In this talk, I will discuss SEDs coming from the FirstLight database of cosmological simulations of first galaxies at cosmic dawn, $z = 5 - 15$ (Ceverino, Glover, Klessen 2017). These cosmological simulations provide complex SFHs that are coupled with the non-uniform gas accretion history of galactic halos (Section 2 and Ceverino, Klessen, Glover 2018). The simulated SEDs are therefore consistent with the cosmological growth of structures at early times (Section 3). The final section discusses some results that can be found at Ceverino *et al.* (2018), such as BPT diagrams.

2. Dwarfs at Cosmic Dawn ($z = 6 - 15$)

Galaxies at cosmic dawn look very compact (Fig. 1). The stellar half-mass radius of this example is only 0.5 kpc. This is a factor 10 smaller than local galaxies with a similar mass. They are gas rich and they have typical SFR $\simeq 20\, M_\odot\, \mathrm{yr}^{-1}$, a factor 10 higher than their counterparts at $z = 0$. This drives a clumpy and turbulence gas morphology, more similar to local starbursts. We have used the FirstLight database to study the Star Formation (SF) histories of ∼300 galaxies with a stellar mass between $M_* = 10^6$ and $3 \times 10^9 M_\odot$ during cosmic dawn ($z = 5 - 15$).

The evolution of the SFR in each galaxy is complex and diverse, characterized by bursts of SF. Overall, first galaxies spend about 70% of their time undergoing SF bursts at $z > 5$. This diversity sets the mean and scatter of the SFMS at $z \simeq 5 - 13$. High gas fractions and short gas depletion times are common during the SF bursts. The typical

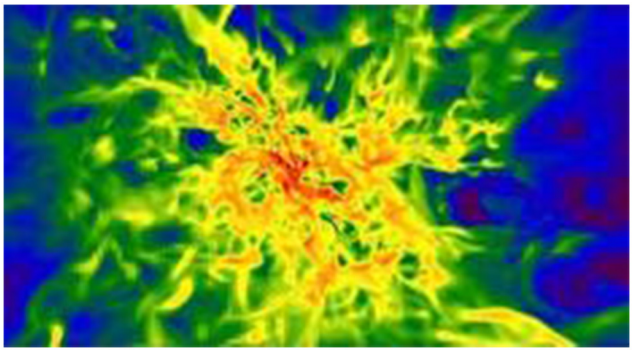

Figure 1. Gas distribution of a dwarf galaxy at $z = 6$. The horizontal size of the image is 4 kpc.

bursts at $z \simeq 6$ have a sSFR maximum of $5 - 15\,\mathrm{Gyr}^{-1}$ with a duration of ∼100 Myr, one tenth of the age of the Universe. A quarter of the bursts populate a tail with very high sSFR maxima of $20 - 30\,\mathrm{Gyr}^{-1}$ and significantly shorter time-scales of $\sim 40 - 80$ Myr at all masses. The mean period of time between consecutive bursts is ∼200 Myr with a small mass dependence at $z \simeq 6$. The mean sSFR increases with redshift approximately as $sSFR \propto (1+z)^{5/2}$ at all masses, as predicted by ΛCDM models. This is consistent with existing observations at $z \leq 8$. The typical sSFR height of a SF burst also increases with redshift, but it is always a factor 2 ± 0.5 higher than the mean sSFR at that redshift. This implies typical sSFR maxima of $sSFR_{\rm max} = 20 - 30\,\mathrm{Gyr}^{-1}$ at $z = 9 - 10$. The tail of the distribution reaches $sSFR_{\rm max} \simeq 60\,\mathrm{Gyr}^{-1}$ at these high redshifts. This evolution is driven by shorter time-scales at higher redshifts, proportional to the age of the Universe. These galaxies are the most efficient star formers in the history of the Universe.

3. Example SEDs

In this talk we focus on the intrinsic SEDs coming from the stellar populations and their surrounding, unresolved HII regions. They provide templates that could be used for a better understanding of the underlying stellar and gas properties in galaxies at cosmic dawn. Therefore, we ignore dust attenuation or any other radiative transfer effect from intervening gas. These effects will be consider in future works. We compute the SEDs of the simulated galaxies using publicly available tables from the Binary Population and Spectral Synthesis (BPASS) model (Eldrige *et al.* 2017) including nebular emission (Xiao *et al.* 2018).

Figure 2 shows two examples which represent the same galaxy with a stellar mass of $M_* \simeq 10^8 M_\odot$ at $z \simeq 6$, at two different phases of evolution. The left panel depicts the galaxy at the peak of a burst of star formation. The starburst brings the galaxy a factor 6 times above the star forming main sequence at that redshift (SSFR=30 Gyr^{-1}). Its luminosity at 1500 $\mathring{A}$ is correspondingly high, $M_{1500} \simeq -19$. The nebular emission dominates the SED at all wavelengths. Lines, such as Lyα, Hα, OIII or SiIII, are particularly prominent. For example, the equivalent width (EW) of Hα+NII exceeds 1000 $\mathring{A}$. OIII+Hβ is the next prominent feature with EW$\simeq 700\mathring{A}$. These lines contaminate the continuum in the B and R bands. The nebular continuum is also particularly important in the U band and it is able to completely remove the mass -sensitive Balmer break at 4000 $\mathring{A}$ The stellar continuum is also very steep, consistent with a young stellar population with extremely blue colors, $V - I = -0.2$ and $U - V = -0.4$. These are the typical features of an extreme emission-line galaxy at cosmic dawn. The SED of the same galaxy 200 Myr after the starburst looks very different (right panel of Figure 2). The starburst

https://doi.org/10.1017/S1743921319002175 Published online by Cambridge University Press

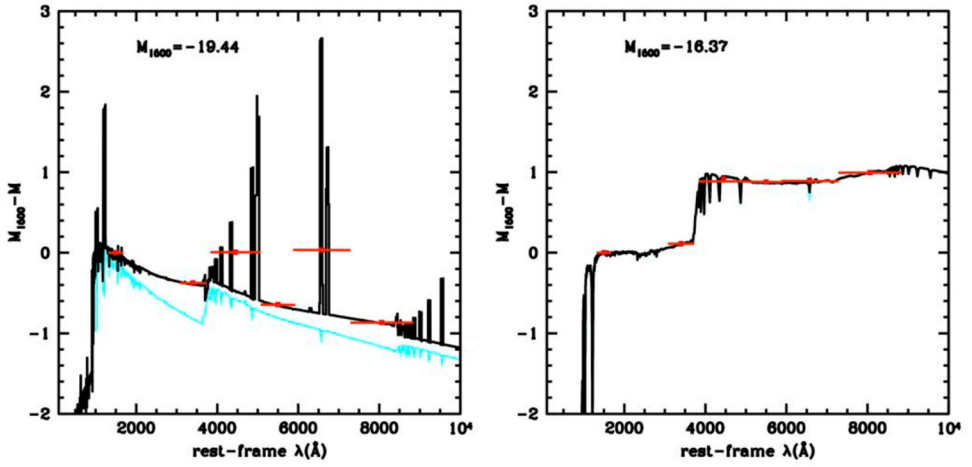

Figure 2. rest-frame SEDs of the same galaxy at the peak of a star formation burst at $z \simeq 6$ (left) and during the subsequent quiescent phase 200 Myr later (right). Cyan lines represent stellar light and black lines include nebular emission (lines+continuum). Red circles with bars represent six photometric bands. The monochromatic luminosity at each wavelength in erg/s/Hz is normalized to the absolute magnitude at 1500 $\mathring{A}$ (top label).

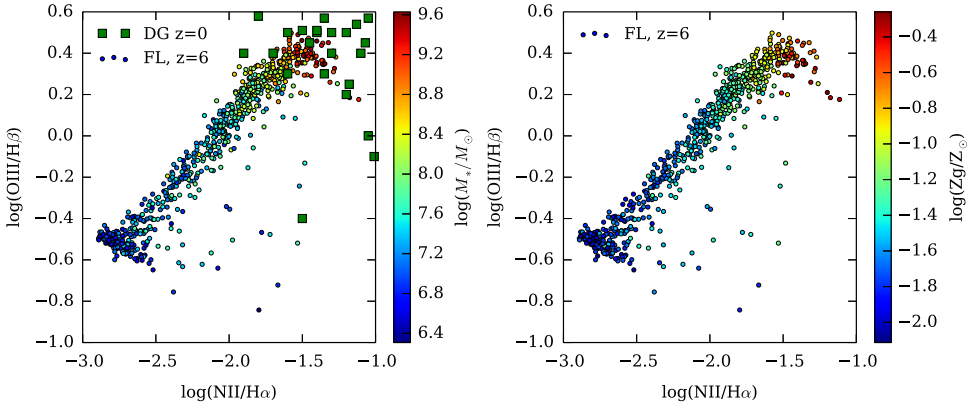

Figure 3. BPT diagrams at $z = 6$ coloured by stellar mass (left), and mean gas metallicity (right). Massive galaxies are consistent with local dwarfs galaxies of similar mass (van Zee & Haynes 2006). Low nebular metallicities drive the sequence towards very low metal-line luminosities.

and the subsequent feedback have quenched star formation significantly (SSFR = 0.02 Gyr^{-1}), placing the galaxy well below the star-forming main sequence. The SED confirms this quiescent nature. The luminosity at 1500 Å is very low, $M_{1500} \simeq -16$, for that stellar mass. There is no significant nebular emission. Instead, there is a strong Balmer break with significantly red rest-frame colors, $V - I = 0.2$ and $U - V = 0.8$, typical of a mature population.

4. BPT Diagrams

The nebular emission lines give some clues about the properties of the HII regions in galaxies using line luminosity ratios like OIII(5007 $\mathring{A}$)/Hβ and NII(6584 $\mathring{A}$)/Hα. In Figure 3 we make predictions of BPT diagrams. The FirstLight galaxies form a clear sequence at $z = 6$. The most massive galaxies, $M_* \simeq 1 - 2 \times 10^9$ $\mathrm{M}_\odot$ occupy the tip of

https://doi.org/10.1017/S1743921319002175 Published online by Cambridge University Press

the sequence with OIII/H$\beta \simeq 0.5$ dex and NII/H$\alpha \simeq -1.5$ dex. These values are consistent with the line ratios of typical HII regions in low-metallicity dwarf galaxies at $z = 0$ (van Zee & Haynes 2006). These regions have relatively high luminosities in OIII with respect to Hβ. Therefore, strong OIII-emitters at low-z could be good analogs of galaxies responsible for reionization (Fletcher *et al.* 2018), although none of our galaxies reaches the highest values of OIII/H$\beta \simeq 1$ dex found in some of these analogs. This is mostly due to the low-metallicity of the primeval galaxies.

Low-mass galaxies have low luminosity ratios, reaching extremely low values for $M_* \simeq 10^6$ M$_\odot$: OIII/H$\beta \simeq -0.5$ dex and NII/H$\alpha \simeq -2.75$ dex. This is mostly driven by the low nebular metallicities of these low-mass galaxies (right panel of Figure 3), which reach $\log(Z_g/Z_\odot) = -2$ for the smallest galaxies in the sample. More massive galaxies, $M_* \simeq 10^8$ M$_\odot$, still have lower ratios than z=0 galaxies due to their low (10% solar) metallicities.

References

Ceverino, D., Glover, S. C. O., & Klessen, R. S. 2017, *MNRAS*, 470, 2791
Ceverino, D., Klessen, R. S., & Glover, S. C. O. 2018, *MNRAS*, 480, 4842
Ceverino, D., Klessen, R., Glover, S. *et al.* 2018, arXiv:1810.09754
Eldridge, J. J., Stanway, E. R., Xiao, L., McClelland, L. A. S., Taylor, G., Ng, M., Greis, S. M. L., Bray, J. C., *et al.* 2017, Publ. Astron. Soc. Australia, 34, e058
Fletcher, T. J., Robertson, B. E., Nakajima, K., Ellis, R. S., Stark, D. P., Inoue, A., *et al.* 2018, preprint, p. arXiv:1806.01741
Kauffmann, G. *et al.* 2003, *MNRAS*, 346, 1055
Xiao, L., Stanway, E. R., Eldridge, J. J., *et al.* 2018, *MNRAS*, 477, 904
van Zee, L. & Haynes, M. P. 2006, *ApJ*, 636, 214

Discussion

Raphael Sadoun: Galaxies in your simulations have a higher star formation rate at z∼12 than at z∼6. Is this due to the fact that your simulations only include thermal feedback by supernovae?

Daniel Ceverino: No, the simulations include thermal, radiative, and kinetic feedback. The increase of the SFR at a fixed mass with redshift is driven by the evolution of the cosmological gas accretion onto halos. Any cosmological simulation should show this evolution at z≥6.

Helen Kim: Why is it that the star-forming galaxies do not follow the star-forming sequence of Kauffmann *et al.* (2003) on the BPT diagram?

Daniel Ceverino: The steep decrease in metallicity (down to 1% solar) for low-mass galaxies ($M_* \sim 10^6 M_\odot$) drives the star-forming sequence towards very low metal line ratios.

Viviana Acquaviva: You showed us that the FIRSTLIGHT simulations can successfully reproduce several observational properties such as star formation rates and line ratios. Is there something that the simulation cannot reproduce well?

Daniel Ceverino: The UV slope β of bright galaxies ($M_{UV} < -19$) is inconsistent with observations because dust is not included in our spectral energy distributions. This would be addressed in future follow-ups.

https://doi.org/10.1017/S1743921319002175 Published online by Cambridge University Press